Behavior of rare earth elements in an aquifer perturbed by CO2 injection: Environmental implications

Jean Rillard, Olivier Pourret, Paolo Censi, Claudio Inguaggiato, Pierpaolo Zuddas, Pierre Toulhoat, Philippe Gombert, Lorenzo Brusca

Title: **Behavior of Rare Earth Elements in an Aquifer Perturbed by CO_2 Injection : Environmental Implications**

Highlights

- The behavior of dissolved REE in groundwater within the critical zone is difficult to evaluate
- Behavior of REE and trace metals was studied upon an aquifer perturbated by CO_2 injection
- A geochemical model was used to evaluated dissolved REE behavior
- REE complexation is/are the main factors controlling REE release and fractionation
- REE fractionation can be used to predict bulk water-rock interaction

Authors : Jean Rillard[1], Olivier Pourret[2], Paolo Censi[3], Claudio Inguaggiato[4], Pierpaolo Zuddas[5], Pierre Toulhoat[6], Philippe Gombert[7], Lorenzo Brusca[8]

[1] BRGM, 5 rue de la Goelette 86280, Saint Benoit, France

[2] UniLaSalle, AGHYLE, 19 rue Pierre Waguet, 60026 Beauvais, France

[3] Department of Earth and Marine Sciences, University of Palermo, Via Archirafi, 36, 90123 Palermo, Italy

[4] Departamento de Geología, Centro de Investigación Científica y de Educación Superior de Ensenada (CICESE), Carretera Ensenada-Tijuana 3918, Ensenada, Baja California, México

[5] Sorbonne Universités, UPMC Univ. Paris 06, CNRS ISTEP, 4 place Jussieu, 75005 Paris, France

[6] BRGM, 3 av. Claude Guillemin 45060 Orléans, France

[7] INERIS, Parc Technologique Alata, 60550 Verneuil-en-Halatte, France

[8] INGV National Institute of Geophisics and Volcanology, Section of Palermo, Via U. La Malfa, 153, 90146 Palermo, Italy

Keywords :

Rare Earth Elements, CO_2 perturbation, REE model complexation, lanthanide tetrad effect, field experiment, Critical zone

Abstract

Three cubic-meters of CO_2-saturated water was injected into a subsurface fractured aquifer in a post-mined area, using a push-pull test protocol. Groundwater samples were collected before and after CO2-injection to quantify geochemical changes. CO_2-injection initially reduced the pH from 7.3 to 5.7, led to the enrichment of major ions (Ca^{2+}, Mg^{2+}, and alkalinity), and dissolved trace metals (including Fe, Mn, As, and Zn) in the groundwater. Rare earth elements (REE) and yttrium concentrations were also measured in these samples before and after CO_2 perturbation, to evaluate their behavior. An enrichment of total Y plus REE (REY) occurred. REY fractionation was observed with higher heavy REE (HREE) enrichment compared to light REE (LREE), and significant variations in La/Yb and Y/Ho ratios were observed following CO_2 perturbation. Enrichment by a factor of three was observed for Y, Lu, and Tm, and by nearly one order of magnitude for Dy and Yb. A geochemical model was used to evaluate the amount of REE aqueous ions complexed over the experiment. Modeling of the results showed that speciation of dissolved REE with carbonate, and desorption from an iron oxyhydroxide surface were the main factors controlling REE behavior. This study increases an understanding of dissolved REE behavior in the environment, and the potential use and limitations for applying iron oxides for REE recovery from mine drainages. Furthermore, the description of REE fractionation patterns may assist in surveying CO_2 geological storage sites, surveying underground waste disposal sites, and for understanding the formation of ore deposits and fluid inclusions.

Introduction

The behavior of rare earth elements (REEs) in natural environments has been extensively studied (Michard 1989; Johannesson et al. 1995, 1997; Choi et al. 2009; Noack et al. 2014). REEs are valuable as components in electronic and renewable energy technologies. The European Community classifies REEs as critical raw materials (European Community, 2010, 2017).

An understanding of REE mobility, their accumulation, and their global cycling mechanisms in the natural environment, is important for evaluating their reserves for future use (Pourret and Tuduri 2017), and to anticipate environmental issues involved in the intensive exploitation of these materials (Filho 2016; Edahbi et al. 2018a).

Extraction of REEs and associated critical elements have been optimized using in-situ leaching techniques to enhance their extraction rates (Haschke et al. 2016; Vahidi et al. 2016). Dissolved REE fractionation patterns have been used as a proxy for understanding many geodynamic processes, such as magmatic melting and water-rock interactions (Bau 1996, 1999; Irber 1999). Dissolved REE studies also suggest methods for tracing the environmental impacts of human activity, including shale gas hydraulic fracturing fluid analysis (Yang et al. 2018). The physico-chemical properties of REEs allow

60 them to be used as robust proxies for studying low and high-temperature geochemical reactions
61 (Pérez-López et al. 2010; Hannigan and Sholkovitz 2001).

62 The geological storage of CO_2, which is part of carbon capture and storage (CCS) technology, has been
63 considered a potential method for reducing the accumulation of atmospheric greenhouse gases (IPCC
64 2005). Geological storage involves injecting CO_2 previously captured from industrial processes into
65 deep underground rock formations. The aim of doing so is to permanently remove CO_2 from the
66 atmosphere. The effectiveness of storage depends on the reservoir storage site's capacity and
67 integrity. CO_2 storage capacity is driven by porosity, reservoir permeability, and the existence of a
68 sufficient impermeable barrier or cap rock for containing the CO_2 permanently. Several types of
69 geological formations have been identified as having a suitable capacity for CCS. To date, these
70 reservoirs include deep saline aquifers, coal bed formations, oil and gas reservoirs exploited through
71 enhanced oil recovery technics using CO_2, and finally, depleted oil and gas reservoirs. Among these
72 storage sites, deep saline aquifers have been identified for having larger storage capacity and
73 worldwide distribution (Bachu et al. 2007).

74 Once injected, part of the CO_2 will be physically trapped beneath the impermeable cap rock, which
75 acts as a seal, and the remaining CO_2 will dissolve into the aqueous phase. Part of this dissolved CO_2
76 may react with reservoir rocks to form a new mineral (CO_2 mineral trapping), or alternatively, may
77 remain dissolved into the aqueous phase (solution trapping) (Bachu et al. 1994). As such, an
78 understanding of CO_2-water-rock interaction processes are of primary importance for validating the
79 feasibility and effectiveness of CCS. To study this phenomenon, numerous experiments have been
80 performed under laboratory conditions alongside geochemical models (Little and Jackson 2010; Liu et
81 al. 2012; Humez et al. 2013; Pearce et al. 2015). Modeling of experimental data offers accuracy for
82 chemical reaction descriptions, but is fairly limited in terms of time and scale. The study of natural CO_2
83 hydrothermal-rich water offers good analogues for studying long-time CO_2-water-rock interaction, but
84 appears limited in its ability to describe chemical phenomena with a good degree of precision (Gilfillan
85 et al. 2009; Keating et al. 2010; Gal et al. 2012). Several field experiments have been performed as pilot
86 tests for identifying the scale of CCS sites, and to identify technical and scientific gaps (see Jenkins et
87 al. 2015, and references therein).

88 The above-noted experimental works have shown that several issues must be resolved, including the
89 environmental risks involved in CCS processes. Several preliminary experiments, in the field and in the
90 laboratory, suggest the potential risks of releasing dissolved trace metals into subsurface freshwater
91 aquifers. The release of dissolved metals may be caused by CO_2-enriched brine leaking from an initial
92 deep storage reservoir, and moving toward the surface. Among other phenomena, the remobilization

of trace metals is related to in-situ pH and redox perturbations involved in CO_2-injection or leakage. In particular, CO_2 perturbation may involve pH acidification, thereby enhancing dissolution of the reservoir rock, and generating the release of trace metals that may initially be present in the reservoir rock minerals, or that have been sorbed onto mineral surfaces (Kharaka et al. 2006; Little and Jackson 2010; Wilkin and Digiulio 2010; Siirila et al. 2012; Wunsch et al. 2013; Rillard et al. 2014; Jenkins et al. 2015). Understanding the fate and transport of trace metal elements in subsurface geological environments is therefore important. These issues are also valuable for other geoengineering applications such as toxic waste disposal, long-term underground storage of radioactive waste, and monitoring of waste landfills.

CO_2-water-rock interactions are driven by the crystallization of newly-formed minerals at the fluid-rock interface. Thus, the feasibility of CO_2 storage is based on a surface-driven process and elements of the lanthanide series which, along with yttrium, represent a promising geochemical tool for describing processes occurring at the interface between injected fluids and host rock. The behavior of REY in groundwater may help to understand the reactions occurring at the water-rock interfaces following interaction with injected CO_2.

Shand et al. (2005) highlight that the concentration of dissolved REE in groundwater is controlled by several factors. These include the release of chemical elements resulting from weathering processes, groundwater pH and redox reactions, adsorption processes, complexing ligands in groundwater, and physical hydrogeological factors (hydrodynamic processes and residence time). Studies of dissolved REE behavior within geothermal fluids and natural CO_2-rich water sources have produced useful results. A fractionation pattern for REEs occurs during CO_2, water, and rock interaction processes, and a strong relationship has been identified between dissolved REEs and water pH (Lewis et al. 1998; Michard 1989; Shand et al. 2005; Inguaggiato et al. 2015). The use of REEs as tracers of high salinity brine leakage detection in CCS applications has been studied under laboratory conditions (McLing et al. 2014). However, several issues were presented, such as the high salinity content of samples, which caused analytical problems for trace metal analyses.

REE signatures in fluid inclusions is also a key parameter for enhancing an understanding of the behavior of deep geological fluids. In particular, REE fractionation patterns are good proxies for evaluating the physico-chemical conditions, fluid-mixing, and precipitation processes operating during the genesis of valuable geological resources, such as oil, gas, and ore deposits (Zwahlen et al. 2019; Shu and Liu 2019; Perry and Gysi 2018).

During mineral crystallization, REEs behave as a function of their ionic charge and radius (charge and radius controlled (CHARAC) processes; see Bau 1996). During aqueous processes, however, these

metal cations react based on their external electronic configuration. As such, the main change in the features of normalized REE concentrations, and in the Y/Ho ratio, can be recognized through interactions at the rock-fluid interface (Bau et al. 1998, 2003; Irber 1999; Negrel et al. 2000; Takahashi et al. 2002). Of special importance is the scavenging of REEs by metallic oxide and hydroxide phases (i.e. oxyhydroxides such as iron and manganese oxyhydroxides), which affects the form of REEs in aqueous media (De Carlo et al. 1998; Quinn et al. 2006; Schijf and Marshaal 2011; Liu et al. 2017). Complexation of REEs onto iron and manganese oxides is strongly pH-dependent (Bau 1999; Verplanck et al. 2004; Quinn et al. 2006, 2007). The binding of these cations to an amorphous phase such as ferrihydrite (e.g. $Fe(OH)_3$) is important, due to the large reactive surface area. Using zerovalent iron nanoparticles for REE recovery from acid mine drainage under laboratory conditions showed the ability of these oxyhydroxide minerals to remove REEs from a solution (Crane and Sapsford 2018). Fractionation between light REEs (LREEs) and heavy REEs (HREEs) occurs during scavenging onto metal oxides. This is primarily driven by dissolved species complexation, particularly in the presence of carbonate species (De Carlo et al. 1998; Bau 1999; Ohta and Kawabe 2001; Quinn et al. 2007; Schijf and Marshall 2011; Munemoto et al. 2015). Many studies have evaluated REE complexation with organic and inorganic ligands. The complexation process of REEs occurring on mineral or organic surfaces is key to understanding the behavior of dissolved REE patterns in the environment (Wood 1990; Tang and Johannesson 2003; Pourret et al. 2007; Pourret and Martinez 2009; Pourret et al. 2010).

Understanding dissolved REEs' behavior is challenging, due to the involvement and interdependence of the phenomena described above. The aim of this experimental work is to study the potential enrichment of dissolved trace metals and REY in groundwater perturbated by CO_2, and its potential application to CO_2 geological storage safety site assessment. An existing study employing this experiment focused on major chemical elements and trace metal remobilization for studying the potential environmental issues involved in CCS (Rillard et al. 2014). A second set of samples, collected during the same fieldwork, was used to study the behavior of dissolved REE. The aim of the present study is to quantify the effect of CO_2 and pH-perturbation of the aquifer on release of dissolved REY. This work may enhance an understanding of the fate and transport of dissolved REEs and associated trace metals into the environment, for evaluating the safety of geological CO_2 storage. The results may also be useful for other geoengineering applications, including the geological storage of radioactive waste and mine site remediation.

1. Geological and hydrogeological site setting

The detailed geological and hydrogeological settings of the experimental site is described in Rillard et al. (2014). The experimental site is located in the Lodève area, Southern France, roughly 80 km north of Montpellier. The local geology involves large Permian sandstones and shales lying on top of Cambrian dolomites. Sandstones are dark-red in color, due to high concentrations of iron hydroxides, while shales are characterized by grey coloring, due to their high organic matter content. The experiment site is situated within a 400 m-thick sandstone and shale formation. From the 1950s to the early 1990s, this area had been extensively mined for uranium and arsenic using underground galleries and open pit mines, due to the high concentration of trace metals in the bedrock.

Denser mineralized deposits representing higher concentrations of metals can be found in vein deposits throughout the fractured network. The mineralization processes have been attributed to hydrothermal fluid circulation and associated secondary mineral precipitation (Brockamp and Clauer 2013; Laurent et al. 2017). The primary mineralogical association between arsenic and uranium refers to arsenuranospathite deposits (Dal Bo et al. 2015). This area is also characterized by hydrothermal activity, with hot springs that are sometimes naturally enriched with CO_2, and locally exploited for geothermal energy (Bonnaveira et al. 1999).

The sandstone and shale formations are characterized by low permeability (estimated by a pumping test at 10^{-7} m.s^{-1}) and low total porosity (estimated at less than 5%). Groundwater circulation mainly occurs via a network of rock fractures.

The following average modal composition of major minerals in the host-rock was determined: dolomite (20%), albite (20%), K-feldspar (30%), quartz (15%), illite (10%), other (5% calcite and iron oxihydroxide, siderite, and pyrite) (Brockamp and Clauer 2013; Chopin 2016). However, mineral compositions may vary among different strata. Indeed, significant amounts of neoformed mineral phases were observed along the surface fractures by camera logging, performed immediately after experimental well implementation. In particular, the presence of amorphous iron oxihydroxides was identified as a product of pyrite oxidation (Rillard et al. 2014).

2. Materials and methods

A field experiment using a CO_2-rich water injection was performed following a push-pull test protocol (Haggerty et al. 1998; Istok et al. 1997; Matter et al. 2007). This experiment configuration offered an intermediate scale between laboratory experiments, where chemical reactions can be constrained and accurately described, and larger scale studies in natural CO_2 hydrothermal fields. In the latter, the CO_2 quantity involved and the hydrodynamic processes (mixing, residence time, etc.) is difficult to quantify.

A 115 m-deep well was drilled through the sandstone and shale formations. The well was cemented and equipped with PVC tubing on the uppermost 20 m, in order to avoid contamination from surface and subsurface water. No equipment (or tubing) was installed from 20 m to 115 m deep in order to avoid contamination by well-tubing alteration, as shown in previous works (Kharaka et al. 2006). The entire geological well-log is presented in Rillard et al. (2014). Several hydrogeological prospections (pumping tests, packer test, microflow logging, tracing test, well-logging, physicochemical groundwater logging) were performed to determine the most suitable depth interval for injecting CO_2-saturated water. The injection was performed along a 3 m interval located at a 56 m depth within a fractured zone, through the sandstone layer. This injection zone was isolated using a double-packer system.

A 3 m^3 volume of baseline groundwater was initially pumped from the isolated well interval, temporarily stored in a water tank, and then saturated with pure CO_2 using a bubbling system. Once CO_2-saturation was reached (determined by a stable pH of 5.7, from an initial value of 7.3), the 3 m^3 volume was injected through the packer system, following a single-well push-pull test protocol (Haggerty et al. 1998; Istok et al. 1997; Matter et al. 2007). Samples were collected into the water tank before and after CO_2-saturation in order to determine baseline groundwater composition. An elapsed time of 80 h was employed following the injection phase, to provide a sufficient interaction time between the injected solution and the host rock. This 'interaction' time was followed by a 80 h pumping period to re-pump the 3 m^3 injected volume, plus the mixed-formation water. This protocol was adapted from studies by Haggerty et al. (1998), Istok et al. (1997), and Matter et al. (2007).

Samples were systematically collected over the entire pumping period to evaluate the impact of CO_2 perturbation on groundwater chemical composition. A sampling protocol using a glovebox and inert plastic bottles, previously filled with nitrogen gas, was used to minimize sample oxidation and contamination. Samples used for metal analysis were filtered in the field using a 0.2 µm filter, and acidified using HNO_3 Normapur (70%), until reaching a pH<2. A second set of samples was filtered in the field using a 0.45 µm filter for major cations and anions analysis. Physicochemical parameters, pH, conductivity, temperature, and redox potential were continuously monitored using a flow-through cell, installed at the top of the well during the injection and pumping phase. Fe (II) was measured in the field for individual samples collected, using a portable spectrophotometer-specific IRON(II) LR® reagent. Alkalinity was measured in the field by HNO_3 acid titration of regularly-collected individual samples.

A list of the samples used for specific REE analyses is presented in Table 1. The corresponding pH, redox potential, and conductivity measured in the field, and the pumped volume on injected volume ratio

illustrates the pumping stage evolution corresponding to each individual sample. Samples one to 19 were collected at different intervals during the pumping phase. Sample one was collected a few minutes after the start of pumping. Sample 19 was collected roughly 24 h after the start of pumping.

The analysis for REEs and several additional trace elements was performed at the Istituto Nazionale di Geofisica e Vulcanologia (INGV) geochemical laboratory in Palermo, Italy. REEs were analyzed by Q-ICP-MS (Agilent 7500ce). A mass spectrometer was calibrated in the range of 5-5000 ng/L, with 11 calibration points obtained by stepwise dilution of a REE multi-element standard solution. The sensitivity variations were monitored using internal standards ^{103}Rh, ^{115}In, and ^{185}Re, which were added directly online by an appropriate device, by mixing an internal standard solution to the sample immediately before the nebulizer. A 60 s rinse using a 2% HNO_3 solution and 0.5% HCl solution, plus a 60 s rinse using a 2% HNO_3 solution reduced memory interferences between samples. Standards and samples were replicated five times to evaluate the data precision by relative standard deviation (RSD), which was always <15%. The standard reference materials SLRS4 (Lawrence et al. 2006), and SpectraPure Standards SW1 and SW2 were analyzed to evaluate data accuracy, which never exceeded 10%.

3. Speciation model with PHREEQC

To understand the parameters controlling REE behavior as a result of CO_2-injection, a geochemical model was used, with particular attention paid to sorption/desorption processes and speciation phenomena.

The speciation modeling for Fe-oxide equilibrium calculations was achieved using hydrogeochemical code PHREEQC ver. 3.3.9 (Parkhurst and Appelo 2013), as well as the wateq4f database. This database was updated using the well-accepted stability constants for the 14 naturally occurring REEs at zero ionic strength, and at 25°C. These constants account for inorganic aqueous complexes with carbonate, hydroxyl, sulfate, chloride, and fluoride anions. The stability constants for $LnCl^{2+}$ and $LnCl_2^{+}$ were taken from Luo and Byrne (2001), and $LnF^{2+}$and LnF_2^{+} were taken from Luo and Millero (2004). Those for $LnSO_4^{+}$ were obtained from Schijf and Byrne (2004), and those for $LnNO_3^{2+}$ from Millero (1992). Constants for $Ln(OH)^{2+}$ and $Ln(OH)_2^{+}$ were taken from Lee and Byrne (1992), and those for $Ln(OH)_3(a)$ from Klungness and Byrne (2000), respectively. Equilibrium constants for the formation of $LnCO_3^{+}$ and $Ln(CO_3)^{2-}$ were taken from Luo and Byrne (2001). Scavenging model parameters for HFO were taken

from Liu et al. (2017). Precipitation of HFO was quantified from dissolved Fe measured in groundwater samples, and the corresponding equilibrium constants were taken from Nordstrom et al. (1990). The number of REE binding sites in the reactive solid surfaces was determined by the moles of HFO, precipitated and defined explicitly by the keyword data block 'EQUILIBRIUM PHASES'. The specific surface area (SSA) was defined relative to the moles of HFO, in which the amount of specified binding sites changed as the SSA varied during the batch-reaction simulation. Upon HFO formation, the two types of oxide surface binding sites (= S^sOH and = S^wOH) were assumed to be available for REE complexation. For surface complexation modeling, both the surface-bound and diffuse layer species were taken as components of the system in the presence of iron oxyhydroxides. In this modeling configuration, iron hydroxides were only considered as solid phase (i.e., colloid or mineral phase).

All of the REEs considered in the model were trivalent, and followed the hypothesis of Bau (1999) that oxidation-scavenging of Ce by metal oxides included three independent steps: (1) sorption of Ce(III) from solution; (2) partial oxidation of Ce(III) to Ce(IV) on the iron or manganese oxide surface; (3) partial desorption of Ce(IV) to solution.

4. Results

4.1 REY enrichment and fractionation following CO_2 perturbation

The physicochemical parameters (pH, redox, and conductivity) measured in the field during the experiment are listed in Table 1 and represented in Fig. 1 as functions of the ratio of pumped volume to injected volume (i.e. Vp./Vinj.). The evolution of iron and manganese, as major reactive metals following the CO2-injection, is represented in Fig.2a. Other parameters that may influence REY behavior such as aluminum content did not show clear evolution following CO_2 perturbation. Dissolved organic carbon (DOC), as well as total organic carbon (TOC), were below the detection limit for all samples. A clear increase for As and Zn was correlated with CO_2 perturbation. The specific behavior of these elements, as well as other major parameters (Ca^{2+}, Mg^{2+}; alkalinity, etc.) are presented in detail in Rillard et al. (2014). Only parameters that have been identified as having an impact on REY behavior were studied in the present paper.

In this study, the entire REEs series plus Y was analyzed; however, only REEs used in the geochemical model (see part 3) were employed. A small number of representative elements per group of REEs is presented in molar concentration as a function of Vp./Vinj. ratio (see Fig.3): Ce for the LREE group, Gd and Dy for MREE, and Yb and Y for HREE. A Vp./Vinj. ratio close to zero represents the beginning of the pumping stage, and the most CO_2-perturbed sample. A global enrichment in REY concentration was

observed following CO2-injection (Fig.3). The ∑REY increased from $1.2 \cdot 10^{-9}$ mol/L to $4.3 \cdot 10^{-9}$ mol/L, following a pH decrease (Fig.4). Higher enrichment was observed for Y (from $8.1 \cdot 10^{-10}$ mol·L^{-1} to $3.2 \cdot 10^{-9}$ mol·L^{-1}) (Fig.3, Y image). Global REE enrichment following CO_2 perturbation was induced by acidification related to carbonic acid production. Acidification enhanced host rock mineral weathering, releasing trace metals into the aqueous phase. Global REY enrichment mimics the global increase in dissolved metals, such as iron and manganese (see Fig.2, and Rillard et al. 2014). This was evident when comparing the baseline groundwater composition (baseline groundwater sample) to the most perturbed CO_2 sample (sample one). However, the enrichment was not homogeneous along the entire REEs spectrum. Enrichment in dissolved REEs and global correlation with CO_2 perturbation appeared greater for Y and HREE (Fig.3). Good correspondence between dissolved concentration and CO_2 perturbation was observed for Y, Dy, Er, Tm, Yb, Lu, Gd, and Tb (i.e. MREE and HREE). A regular increase in the concentration of ∑HREE (plus Y) occurred alongside a pH decrease, as a result of CO_2 perturbation, until the end of the pumping phase, as shown in Fig. 4. The increase in MREE appeared less-marked as a function of pH and Vp./Vinj (Fig. 4). In contrast, no systematic evolution was observed for LREE as a function of pH and Vp./Vinj.

Typical REE parameter (La/Yb, Ce/Ce*) evolution as a function of Vp./Vinj. is shown in Fig. 5. The La/Yb ratio shows an abrupt decrease following CO2-injection, and a smooth increase toward the baseline water ratio after Vp/Vinj. reached 0.5. No clear evolution was apparent for Ce/Ce* as a function of Vp/Vinj. A decrease in Ce anomaly appeared to have occurred immediately after CO2-injection, but no clear trend was observed as a function of Vp./Vinj. The fractionation of HREE compared to LREE appeared quite clear and was also confirmed by the evolution of La/Yb ratio as a function of Vp./Vinj. (Fig.5). The Eu/Eu* anomaly was not considered, since interference with BaO during analysis was suspected (Shabani et al. 1992; Dulski 1994; Zwahlen et al. 2019). Despite the absence of a clear correlation between Ba and Eu (see supplementary materials), the ratio Eu/Ba was >4000, and this may have led to a false positive Eu signal.

The entire REE pattern of the experimental samples, normalized to PAAS (Post Archeen Australian Shale), is shown in Fig.6a. In order to simplify the visual result, only the most representative experimental samples are presented: baseline groundwater; Vp.Vinj. = 0, representing the most perturbed sample; Vp./Vinj. = 0.033 was the second most perturbed sample; Vp./Vinj. = 1.489 was representative of a sample collected at the end of the pumping phase. Data for Eu are not shown, since interference with Ba was suspected, as discussed above. The REE pattern showed a net enrichment of HREE in both the baseline groundwater composition (baseline groundwater sample), following CO_2-injection. This trend did not change significantly due to CO_2 perturbation. However, the fractionation of HREE was significant following CO_2 perturbation. For comparison, the entire REE pattern normalized

to PAAS for bulk rock samples analysis is also presented in Fig 6b. These samples were collected on the same shale and sandstone formation as the experimental site in this study (data issued by Chopin 2016). The normalized to PAAS concentration of the bulk rock shows a clear enrichment of HREE compared to LREE, in correlation with the general trend of REE observed for water samples. However, a weak MREE enrichment (particularly for Gd, Tb, and Dy), compared to LREE was observed. This point was not clearly indicated in the water samples. However, the amplitude of this enrichment in MREE concentration remained limited (lower than 0.2).

4.2. REE speciation

REE speciation calculation results are shown in Fig. 7. The baseline water plot represents the baseline groundwater sample, while sample one, with the lowest pH, represents the earliest sample collected following CO_2 perturbation. The total proportion of REE complexes (%Ln3+; %LnCO3+ (CO3)2; %LnSO4; %LnHFO) are represented as a function of pH and Vp./Vinj. ratio (see Fig.8).

The dissolved REE-carbonate complex is indicated as the dominant species prior to CO_2 perturbation (Fig. 7, baseline groundwater sample). The proportion of REE complexation with carbonate was nearly homogenous along the entire REE pattern, with no particular fractionation effects. REEs sorbed to iron oxyhydroxide (Fig.7, Ln-HFO) indicates the second highest proportion in baseline groundwater composition. The proportion of Ln-HFO complex increased with atomic weight along the REE series, with a higher proportion of HREE sorbed, compared to LREE, for all samples. The proportion of REE-sulfate complex (Ln-SO_4^+) appeared low compared to the proportion of carbonate complex. A similar observation was made for free REE ions (Ln^{3+}).

Following CO_2 perturbation (see Fig.7, sample one, and Fig. 8), the REE-sulfate complex became the dominant species, except for Tm, Yb and Lu, for which the REE-carbonate was the dominant species. The proportion of Ln-SO_4 complex decreased regularly alongside REE atomic weight, and the opposite trend was observed for REE-carbonate (see Fig. 7, sample one to sample 19). The REE-iron oxyhydroxide complex (HFO) decreased following CO_2 perturbation; this is particularly significant when comparing the baseline groundwater to sample one (Fig. 7). From sample one to sample 19, the Ln-carbonate and Ln-HFO complex proportions increased, and REE-sulfate complex decreased as CO_2 perturbation diminished (Fig. 7). However, the total concentration of sulfate in groundwater did not change significantly following CO_2 perturbation. The baseline concentration in sulfate was relatively high. The sulfate concentration stayed at the same order of magnitude over the entire experiment (within 7 mol/L to $9 \cdot 10^{-3}$ mol/L; see Rillard et al. 2014). A weak variation in SO4 concentration was, however, observed during the experiment, but was attributed to the mixing process, in accordance with hydrogeological information observed in the field (Rillard et al. 2014). The initial high amount of

sulfate in baseline groundwater was attributed to mixing with local groundwater contaminated by former mine activities in the area (influence of acid rock drainage, sulfide mineral oxidation, etc.). Therefore, the higher proportion of Ln-SO_4 following CO_2 perturbation is related to the higher affinity of dissolved REEs for complexing with sulfate in acidic conditions (Decree et al. 2015), but not to an increase in sulfate concentration induced by CO_2 perturbation.

Enrichment of dissolved REEs was greater for Y and HREE. This was clear when comparing the La/Sm ratio normalized to PAAS $(La/Sm)_{N\text{-}PAAS}$, and the $La/Yb)_{N\text{-}PAAS}$ ratio (Fig.5). La/Sm and La/Yb ratios decreased after CO2-injection, due to the higher amounts of HREE and MREE released in the water, compared to the LREE. Similarly, a large increase in the Yb/Gd ratio (from 0.54 to 2.23) was observed following CO_2 perturbation.

5. Discussion

5.1. Effects of CO_2 perturbation on REY enrichment

CO_2 perturbation increased the concentration of major elements (e.g. $Ca^{2+}$and Mg^{2+}) by nearly 30%, and alkalinity doubled (Rillard et al. 2014). The pH initially decreased from 7.3 to 5.7, dissolved Fe rose from $2.15 \cdot 10^{-5}$ mol/L to $1.17 \cdot 10^{-4}$ mol/L, and Mn from $1.35 \cdot 10^{-6}$ mol/L to $5.01 \cdot 10^{-6}$ mol/L. Significant increases in dissolved trace metals, mainly As and Zn, were also observed (Rillard et al. 2014). Redox perturbation throughout the experiment was evaluated by comparing redox potentials measured by electrodes in the field, with those calculated from the Fe (II)/Fe (III) equilibrium. Redox potential was controlled by iron oxyhydroxide equilibrium, but was weakly perturbed and nearly constant throughout the entire experiment (Fig.1).

The main geochemical reactions are identified by the geochemical model. The release of major elements was attributed to weak dissolution and equilibrium of major minerals composing the host rock, particularly dolomite and calcite. The increase in dissolved Fe was attributed to dissolution of amorphous iron oxyhydroxides such as ferrihydrite (Fig. 2b). A good correlation was identified between the saturation index of ferryhidrite and the dissolved iron concentration (Fig.2b). This is also in agreement with the high amount of neoformed iron oxyhydroxide phases observed during drilling operations. The release of dissolved iron is therefore mainly attributed to ferryhidrite dissolution. The enrichment in Mn arose from the dissolution of Mn-oxides, but the specific phase could not be identified using the geochemical model. The enrichment of trace metals, particularly As, is associated with the desorption or dissolution of iron oxyhydroxides. The major factor for the enrichment of trace metals induced by CO_2 is considered to be the acidic pH, derived from carbonic acid production. The perturbation of redox conditions was not considered to be significant (Rillard et al. 2014).

The Ce/Ce* did not show clear evolution as a function of Vp.Vinj. (Fig. 5). The global anomaly of Ce for all samples appeared negative (Tostevin et al. 2016), and a weak decrease appeared to have occurred immediately after CO2-injection, but this is not clearly evidenced in other samples. A cerium anomaly is known for being a good proxy of redox potential variation (Bau and Alexander 2009; Frei et al. 2013; Tostevin et al. 2016). A decrease in cerium anomaly can corroborate an oxidative perturbation. However, the redox potential did not change significantly throughout the entire experiment. The redox potential increased from +130 mV in baseline groundwater to +187 mV following CO_2-injection (Fig.1).

Fig.10 illustrates the Y/Ho molar ratio as a function of Vp./Vinj. ratio. The Y/Ho ratio increased from 57 in baseline groundwater composition to >100 following CO_2 perturbation, before decreasing to <80 when the V p./Vinj. ratio reached 1. The Y/Ho signatures are known to present different behaviors during interactions with Mn and Fe-oxyhydroxides (Bau, 1996, 1999). An increase in Y/Ho ratio was observed following CO_2 perturbation. Such enrichment of Y with respect to Ho was also observed in natural CO_2-rich fluid by Shand et al. (2005). This result, however, is not consistent with the dissolution/desorption of Fe/Mn-oxyhydroxides as the main sources of dissolved REEs. These solids generally preferentially adsorb Ho, relative to Y, during authigenic crystallization (Bau 1999; Bau and Koschinsky 2009). Therefore, the observed Y/Ho variation suggests that another REE-enriched source released REEs into groundwater. This other source may be the desorption of REEs from organic-rich shale surfaces (Haley et al. 2004; Takahashi et al. 2010). Another hypothesis is the dissolution of carbonates or minerals, which may act as a source of anomalous Y (Tostevin et al. 2016). This final hypothesis is consistent with the dissolution of carbonate minerals (such as calcite and dolomite) previously identified as a primary source of Ca^{2+}, Mg^{2+}, and alkalinity release, following CO2-injection (Rillard et al. 2014).

The enrichment in HREE relative to PAAS, within the entire REE series, in both baseline water composition and following CO_2 perturbation, are described in natural CO_2 rich water (Shand et al. 2005), and in volcanic hydrothermal water sources (Inguaggiato et al. 2015, 2016, 2017). These data support the preferential enrichment of HREE during weathering processes induced by CO_2 perturbation. However, as suggested above, some issues regarding analytical precision may have affected some of the results. Due to the very limited volume of water in collected samples (less than 10 mL) and technical limitations, a preconcentration step could not be performed prior to REY analyses with ICPMS. Overall REE concentrations ranged from 1241 pmol/L to 4300 pmol/L. These concentrations are beyond the values in which REE preconcentration and a matrix-free method of analysis are essential. However, the large variation observed in shale-normalized patterns for some samples (the baseline groundwater sample in particular) may have been due to a lack of precision

resulting from chemical analyses. However, this point does not affect the general trend observed for each individual REY element over the entire CO2-injection experiment, as shown in Fig.3 and Fig.4.

5.2 Effects of speciation and surface complexation on REY behavior

Bau (1999) and Verplanck et al. (2004) showed that neoformed iron oxyhydroxides have a higher affinity for HREE scavenging compared to LREE. Therefore, the higher enrichment of HREE may be related to easier dissolution of neoformed hydroxide minerals such as ferrihydrite, following CO_2 perturbation (see Fig. 2, and Rillard et al. 2014). This hypothesis is supported by speciation calculations showing a rapid decrease in the proportion of the Ln-HFO surface complex following CO_2 perturbation (see Fig.7, baseline groundwater sample, sample one, and Fig.8). HREE enrichment is also illustrated in Fig.11, which represents the La/Yb ratio as a function of dissolved Fe concentration. As the pH decreased, enhanced protonation of ferric oxide surfaces occurred, reducing the proportion of negatively charged groups able to complex REE (Bethke, 2007). The modeling configuration only considered the surface complexation onto solid iron hydroxide phases, as calculated in equilibrium, with dissolved iron measured in the samples (this included the colloid or mineral phase comprising the host rock of the aquifer). This model did not take into account solution complexation with iron oxides. Thus, the development of a specific model is needed to study solution complexes with dissolved iron. However, iron is known to easily form large-size colloids in a solution that mainly control REE sorption and speciation (Pourret al. 2007, 2010).

Crane and Sapsford (2018) studied the sorption and fractionation of REE ions with zerovalent iron nanoparticles. The aim of their work was to test the potential of recovering the dissolved REEs contained in an acidic rock drainage solution. Their results showed that HREE had a higher concentration, and faster scavenging, on a neoformed iron oxyhydroxide surface, compared to LREE. Differences in coordination numbers between LREEs and HREEs helped to explain this phenomenon. The differences affected the hydration number, with the number of REE ions decreasing from nine for LREEs to eight for HREEs, with a transition region between Sm to Gd (Wood, 1990). This higher coordination number may therefore preferentially restrict the bulk diffusion of LREE compared to HREE on sorption sites. However, the experimental conditions were significantly different in the work presented by Cran and Sapsford (2018), compared to the present study (use of zerovalent iron with larger pH variation and redox potential).

Furthermore, the global proportion of Ln-carbonate complexes decreased between baseline water (baseline groundwater sample) and the most CO_2 perturbed sample (sample one in Fig.7 and Fig.8). This decrease was less marked for HREE, and similar results were reported by Sholkovitz (1995), Byrne and Sholkovitz (1996), De Carlo et al. (1998) and Bau (1996). The greater stability of HREE carbonate complexes compared to LREE carbonates may explain the preferential release of HREE in water under the experimental conditions of this study.

Speciation calculations show that in the more acidic samples (samples one, two, and three), REE complexes occurred mainly with sulfate ($LnSO_4^+$), along with a higher proportion of complexed LREE (Fig.7 and Fig.8). However, this phenomenon did not involve the obvious enrichment of dissolved LREE. The proportion of REE sulfate complexes may have been overestimated by the model calculation. A higher proportion of REE sulfate complexes under acidic conditions was observed by Decree et al. (2015) and Verplanck et al. (2004).

This speciation model was constructed using the database on speciation constants of REEs available to date. While these constants are well-documented for REE speciation carbonate and iron oxide species, a lack of data remains for other constants dealing with REE speciation in the presence of manganese oxyhydroxides, which may play an important role in dissolved REE behavior (Pourret et al. 2007b; Pourret and Tuduri, 2017; Liu et al. 2017). However, this model was able to provide important information for studying REE complexation with iron oxyhydroxides in Fe-rich groundwater aquifer systems (Verplanck et al. 2004; Quinn et al. 2007; Liu et al. 2017). The complexation with organic molecules (such as humic substances) was not taken into account, since the organic carbon concentration (TOC and DOC) of the samples was below the detection limit. However, organic matter is known to effect important control on REE behavior (Pourret 2007a, 2007b, 2009). Further developments in modeling techniques should incorporate Mn-oxides, organic humic substances, and Fe-oxides simultaneously in a model, in order to better understand the roles of particle colloids in REE mobility in natural systems (Liu et al. 2017).

5.3 Tetrad effect

Employing the tetrad effect (Masuda and Ikeuchi, 1979) can be useful for understanding the behavior of REE on water-rock interaction processes. This is based on shale-normalized patterns divided into four downward convex segments across the entire REE spectrum. A tetrad effect was observed in patterns of the Ln-carbonate complex and REE iron oxyhydroxide complex, represented in samples with pH values ranging between 5.70 and 6.51 (Fig.7). Four upward-curved segments (La-Nd (I), (Pm)-Gd (II), Gd-Ho (III), and Er-Lu (IV) were observed. These patterns are commonly referred to as the M-

type lanthanide tetrad effect (TE) (Masuda et al. 1987; Bau 1996, 1999). The amplitude of the tetrad effect can be used to study the partial dissolution of rock (Bau, 1996, 1999; Irber 1999; Monecke et al. 2002). However, observed M-tetrad effects in Fig.7 were based on modeled complex abundance. It therefore cannot be ruled out that the tetrad effect observed in Fig.7 had been induced by an artifact from speciation modeling. The analytical quality of the data did not allow for quantifying the tetrad effect amplitude with sufficient accuracy. However, the use of the tetrad effect to understand REE behavior through water-rock interactions represents a good perspective for future studies. In particular, the addition of a preconcentration stage will allow for better data accuracy and therefore, better confidence for quantifying the TE, Eu, and Ce anomalies.

Conclusions

A 3 m^3 volume of water saturated with CO_2 was injected into a subsurface fractured aquifer in host rock naturally enriched with trace metals, including REEs. The CO_2-injection into groundwater caused a rapid initial pH decrease (from 7.3 to 5.7), followed by a gradual increase. Chemical changes in the studied system caused by CO_2-injection created significant changes in the geochemical behavior of major elements, trace metals, and dissolved REEs. Enrichment by a factor of nearly four was observed for dissolved REY species. This enrichment was greater for HREE than LREE. The behavior of dissolved REE was evaluated using a geochemical model. Results indicate the main process controlling the release of dissolved REY following CO_2-injection to be the dissolution of iron oxyhydroxides, enhanced by complexation with aqueous carbonate species ($LnCO_3^{2-}$ and $LnCO_3^{-}$). However, the Y/Ho ratio in groundwater suggests that a second source of REEs may have been involved, such as the desorption from carbonate minerals or organic-rich shales.

This study demonstrates the capability of REEs to provide an indication of geochemical interfacial processes occurring at the nanoscale level, during increased interaction between groundwater and host rock, induced by CO_2-injection. This model can help to provide a better understanding of the roles of particle colloids on REEs' mobility in natural systems. These results also present a starting point for evaluation of the environmental impacts of REE exploitation, and for enhancing REE recovery rates using metal oxides under field conditions such as mine drainage. In addition, this study also presents several valuable tools for the understanding of geological fluid-mixing processes, or fluid inclusions formations, which can be useful for understanding deep geological processes.

Acknowledgments

The field experiments were performed with the financial support of INERIS, as a part of the EVARISTE internal research project on the long term impacts of geological CO_2 storage. We thank the Instituto Nazionale di Geofisica e Vulcanologia (INGV) from Palermo (Italy) and Dr. Sergio Bellomo for analytical support. We also thanks Dr Jose Cruz (associate editor) and two anonymous reviewers for their constructives comments that improved the quality of the original manuscript. Dr. Raul E. Martinez is acknowledged for post-editing the English style.

Conflict of interest:

The authors declare no conflict of interest.

References:

Alibo, D.S., Nozaki, Y., 1999. Rare earth elements in seawater: particle association, shale-normalization and Ce oxidation. Geochimica et Cosmochimica Acta 63, 363–372.

Bachu S., Bonijoly D., Bradshaw J., Burruss R., Holloway S., Christensen N.P., Mathiassen O.M., 2007. CO2 storage capacity estimation: Methodology and gaps International Journal of Greenhouse Gas Control, Vol. 1, Issue 4, 430-443.

Bachu S., Gunter W.D., Perkins E.H., 1994. Aquifer disposal of CO2: Hydrodynamic and mineral trapping. Energy Conversion and Management. Vol. 35, Issue 4, 269-279

Bau, M. 1991. Rare-earth element mobility during hydrothermal and metamorphic fluid-rock interaction and the significance of the oxidation state of europium. Chemical Geology, Volume 93, 219-230

Bau M., 1996. Controls on the fractionation of isovalent trace elements in magmatic and aqueous systems: evidence from Y/Ho, Zr/Hf, and lanthanide tetrad effect, Contrib Mineral Petrol, 123, 323–333

Bau M., 1999. Scavenging of dissolved yttrium and rare earths by precipitating iron oxyhydroxide: Experimental evidence for Ce oxidation, Y-Ho fractionation, and lanthanide tetrad effect. Geochimica et Cosmochimica Acta, 63, 67–77

Bau M., Alexander B.W., 2009. Distribution of high field strength elements (Y, Zr, REE, Hf, Ta, Th, U) in adjacent magnetite and chert bands and in reference standards FeR-3 and FeR-4 from the Temagami iron-formation, Canada, and the redox level of the Neoarchean ocean. Precambrian Res., 174 (2009), pp. 337-346

Bau M., Koschinsky A., 2009. Oxidative scavenging of cerium on hydrous Fe oxide: Evidence from the distribution of rare earth elements and yttrium between Fe oxides and Mn oxides in hydrogenetic ferromanganese crusts. Geochemical Journal, 43, 37-47,

Bethke, C.M., 2007. Geochemical and Biogeochemical Reaction Modeling, second ed. Cambridge University Press.

Bonnaveira H., Vasseur G., Dufour Y., Vuillemenot P., 1999. Modélisation d'une anomalie géothermique du Lodévois. Comptes Rendus de l'Académie des Sciences - Series IIA - Earth and Planetary Science, Volume 329, Issue 4, 30 August 1999, Pages 251-256,

Brockamp O., Clauer. O., 2013. Hydrothermal and unexpected diagenetic alteration in Permian shales of the Lodève epigenetic U-deposit of southern France, traced by K–Ar illite and K-feldspar dating. Chemical Geology, 357, 18-28

Byrne R. H., and E. R. Sholkovitz, 1996, Chapter 158 Marine chemistry and geochemistry of the lanthanides, in Handbook on the Physics and Chemistry of Rare Earths , edited by K. A. Gschneidner, Jr. and L. Eyring, vol. 23, pp. 497–593, Elsevier Science.

Censi P., Saiano F., Zuddas P., Nicosia A., Mazzola S., Raso M., 2014. Authigenic phase formation and microbial activity control Zr, Hf, and rare earth element distributions in deep-sea brine sediments. Biogeosciences, 11, 1125–1136. doi:10.5194/bg-11-1125-2014

Crane R.A., Sapsford D.J., 2018. Sorption and fractionation of rare earth element ions onto nanoscale zerovalent iron particles. Chemical Engineering Journal, 345, 126-137. https://doi.org/10.1016/j.cej.2018.03.148

Choi H.S., Yun S.T., Koh Y.K., Mayer B., Park S.S.; Hutcheon I., 2009. Geochemical behavior of rare earth elements during the evolution of CO 2 -rich groundwater: A study from the Kangwon district, South Korea. Chemical Geology, 262, 3, 318-327

Chopin C., 2016. Analyse géochimique de la composition des sediments permiens-triasiques du basin de Graissessac-Lodève traçage des sources. http://rgf.brgm.fr/sites/default/files/upload/documents/production-cientifique/Masters/rgf_amipyr2015_ma13_memoire_chopin.pdf

Cook, P.J., 2014. Geologically Storing Carbon: Learning from the Otway Project Experience. CSIRO Publishing, Melbourne.

Dal Bo F., Hatert F., Baijot M., Philippo S., 2015. Crystal structure of arsenuranospathite from Rabejac, Lode`ve, France. Eur. J. Mineral. 27, 589–597

De Carlo, E.H., Wen, X.Y., Irving, M., 1998. The influence of redox reactions on the uptake of dissolved Ce by suspended Fe and Mn oxide particles. Aquat. Geochem. 3, 357–389.

Decree S., Pourret O., Baele J.M., 2015. Rare earth element fractionation in heterogenite (CoOOH): Implication for cobalt oxidized ore in the Katanga Copperbelt (Democratic Republic of Congo). Journal of Geochemical Exploration 159:290-301. DOI: 10.1016/j.gexplo.2015.10.005

Dulski, P. (1994). Interferences of oxide, hydroxide and chloride analyte species in the determination of rare earth elements in geological samples by inductively coupled plasma‐mass spectrometry. Fresenius' Journal of Analytical Chemistry, 350(4‐5), 194–203. https://doi.org/10.1007/bf00322470

European Community, 2010. Critical raw materials for the EU. Report of the Ad-hoc Working Group on defining critical raw materials. Version of 30 July 2010, 84 p.

European Commission. (2017). Communication from the commission to the European Parliament, the council, the European economic and social committee and the committee of the regions on the 2017 list of Critical Raw Materials for the EU, 8. Retrieved from http://eur-lex.europa.eu/legal-content/EN/TXT/PDF/?uri=CELEX:52017DC0490&from=EN

Filho W.L. 2016. An Analysis of the Environmental Impacts of the Exploitation of Rare Earth Metals. In book Rare Earths Industry, chapter 17, 269-277. DOI: 10.1016/B978-0-12-802328-0.00017-6

Frei R., Gaucher C., Stolper D., Canfield D.E., 2013. D.E. Fluctuations in late Neoproterozoic atmospheric oxidation − Cr isotope chemostratigraphy and iron speciation of the late Ediacaran lower Arroyo del Soldado Group (Uruguay). Gondwana Res., 23 , pp. 797-811

Edahbi M., Plante B., Benzaazaoua M., 2018a. Environmental challenges and identification of the knowledge gaps associated with REE mine wastes management. Journal of Cleaner Production , doi: 10.1016/j.jclepro.2018.11.228

Edahbi M., Plante B., Benzaazaoua M., Ward M., Pelletier M., 2018b. Mobility of rare earth elements in mine drainage: Influence of iron oxides, carbonates, and phosphates. Chemosphere, 199, 647-654

Gal F., Brach M., Braibant G., Bény C., Michel K., 2012. What can be learned from natural analogue studies in view of CO_2 leakage issues in Carbon Capture and Storage applications? Geochemical case study of Sainte-Marguerite area (French Massif Central). International Journal of Greenhouse Gas Control 10, 470-485

Gilfillan S.M.V, Lollar B.S., Holland G., Blagburn D., Stevens S., Schoell M., Cassidy M., ding Z., Zhou Z., Lacrampe-Couloume G., Ballentine C.J., 2009. Solubility trapping in formation water as dominant CO2 sink in natural gas fields. Nature. 458, 614–618

Haggerty, R., Schroth, M.H., Istok, J.D., 1998. Simplified method of "push–pull" testdata analysis for determining in situ reaction rate coefficients. Ground Water 36(2), 314–324.

Haley B. A., Gary P., Klinkhammer G. P., Mc Manus J., 2004. Rare earth elements in pore waters of marine sediments. Geochimica et Cosmochimica Acta, 68, 1265–1279

Hannigan R., Sholkovitz E.R., 2001. The development of middle rare earth element enrichments in freshwaters: Weathering of phosphate minerals. Chemical Geology 175(3):495-508

Haschkea M., Ahmadianb J., Zeidlera L., Hubrig T., 2016. In-Situ Recovery of Critical Technology. Procedia Engineering. 138, 248 – 257 Elements https://doi.org/10.1016/j.proeng.2016.02.082

Humez P., Lagneau V. Lions J., Negrel P., 2013. Assessing the potential consequences of CO_2leakage to freshwater resources: A batch-reaction experiment towards an isotopic tracing tool. Applied Geochemistry, 30, 178-190

Inguaggiato, C., Censi, P., Zuddas, P., Londono, J.M., Chacon, Z., Alzate, D., Brusca, L., D'Alessandro, W., 2015. Geochemistry of REE, Zr and Hf in a wide range of pH and water composition: the Nevado del Ruíz volcano-hydrothermal. Chem. Geol. 417, 125–133. http://dx.doi.org/10.1016/j.chemgeo.2015.09.025.

Inguaggiato, C., Censi, P., Zuddas, P., Londono, J.M., Chacon, Z., Alzate, D., Brusca, L., D'Alessandro, W. (2016). Zirconium–hafnium and rare earth element signatures discriminating the effect of atmospheric fallout from hydrothermal input in volcanic lake water. Chem. Geol. 433, 1–11.

Inguaggiato, C., Garzon, G., Burbano, V., Rouwet, D., 2017. Geochemical processes assessed by Rare Earth Elements fractionation at "Laguna Verde" acidic-sulphate crater lake (Azufral volcano, Colombia). Applied Geochemistry 79:65–74. 10.1016/j.apgeochem.2017.02.013.

IPCC, 2005. IPCC Special Report on Carbon Dioxide Capture and Storage. Prepared by Working Group III of the Intergovernmental Panel on Climate Change, Metz, B., O. Davidson, H. C. de Coninck, M.

654 Loos, and L. A. Meyer. Cambridge University Press, Cambridge, United Kingdom and New York, NY,
655 USA, 442 pp.

656 Irber, W., 1999. The lanthanide tetrad effect and its correlation with K/Rb, Eu/Eu∗, Sr/ Eu, Y/Ho, and
657 Zr/Hf of evolving peraluminous granite suites. Geochimica Cosmochimica Acta 63 (3), 489–508.
658
659 Istok, J.D., Humphrey, M.D., Schroth, M.H., Hyman, M.R., O'Reilly, K.T., 1997. Singlewell "push–pull"
660 test for in situ determination of microbial metabolic activities.Ground Water 4, 618–631.

661
662 Johannesson, K.H., Lyons, W.B., Stetzenbach, K.J. and Byrne, R.H., 1995. The solubility control of rare
663 earth elements in natural terrestrial waters and the significance of PO43− and CO32− in limiting
664 dissolved rare earth concentrations: A review of recent information. Aquat. Geochem. 1, 157-173.

665 Johannesson K.H.,. Stetzenbach K.J.; Hodge V.F., 1997. Rare earth elements as geochemical tracers of
666 regional groundwater mixing. Geochimica et Cosmochimica Acta, 61, 17, 3605-3618
667

668 Jochum KP, Seufert HM, Spettel B, Palme H, 1986. The solar system abundances of Nb, Ta, and Y, and
669 the relative abundances of refractory lithophile elements in differentiated planetary bodies. Geochim
670 Cosmochim Acta 50: 1173–1183

671 Jenkins C., Chadwick A., Hovorka S.D., 2015. The state of the art in monitoring – ten years on.
672 International Journal of Greenhouse Gas Control. 40, 312-349.

673 Keating, E., Fessenden, J., Kanjorski, N., Koning, D., Pawar, R., 2010. The impact of CO2 on shallow
674 groundwater chemistry: observations at a natural analog site and implications for carbon
675 sequestration. Environ. Earth Sci. 60, 521–536.
676
677 Kharaka Y.K., Cole D.R., Hovorka S.D., Gunter W.D., Knauss K.G., Freifeld B.M., 2006. Gas–water–
678 rock interaction in Frio formation following CO2 injection: implications for the storage of greenhouse
679 gases in sedimentary basins Geology, 34, 577-580
680
681 Klungness, G.D., Byrne, R.H., 2000. Comparative hydrolysis behavior of the rare earths and yttrium:
682 the influence of temperature and ionic strength. Polyhedron 19, 99–107.
683
684 Laurent D., Lopez M., Chauvet A., Sauvage A.C., Buatier M, Spangenberg J.E., 2017. Sedimentary
685 fluids/fault interaction during syn-rift burial of the Lodeve Permian Basin (Herault, France): An
686 example of seismic-valve mechanism in active extensional faults. Marine and Petroleum Geology 88,
687 303-328
688
689 Lawrence M.G., Greig A., Collerson K.D., Kamber B.S., 2006. Direct quantification of rare earth
690 element concentrations in natural waters by ICP-MS Applied Geochemistry 21, 839–848
691
692
693 Lewis, A.J., Komninou, A., Yardley, B.W., Palmer, M.R., 1998. Rare earth element speciation in
694 geothermal fluids from Yellowstone National Park, Wyoming, USA. Geochim. Cosmochim. Acta 62,
695 657–663.
696
697 Lee, J.H., Byrne, R.H., 1992. Examination of comparative rare earth element complexation behavior
698 using linear free-energy relationships. Geochimica Cosmochimica Acta 56, 1127–1137.
699

Li, C., Liang, H., Wang, S. and Liu, J. (2018) Study of harmful trace elements and rare earth elements in the Permian tectonically deformed coals from Lugou Mine, North China Coal Basin, China. Journal of Geochemical Exploration 190, 10-25.

Little M.G. , Jackson R.B. , 2010. Potential impacts of leakage from deep CO2 geosequestration on overlying freshwater aquifers Environmental Science & Technology, 44, 23, 9225-9232

Liu H., Pourret O., Guo H., Bonhoure J. 2017. Rare earth elements sorption to iron oxyhydroxide: Model development and application to groundwater. Applied Geochemistry, 87, 158-166, https://doi.org/10.1016/j.apgeochem.2017.10.020

Liu F., Lu P., Griffith C., Hedges S.W., Soong Y., Hellevang H., Zhu C., 2012. CO2–brine–caprock interaction: Reactivity experiments on Eau Claire shale and a review of relevant literature. International Journal of Greenhouse Gas Control 7, 153-167

Luo, Y.R., Byrne, R.H., 2001. Yttrium and rare earth element complexation by chloride ions at 25 C. J. Solut. Chem. 30 (9), 837–845.

Luo, Y., Millero, F.J., 2004. Effects of temperature and ionic strength on the stabilities of the first and second fluoride complexes of yttrium and the rare earth elements. Geochimica cosmochimica acta 68 (21), 4301–4308.

Masuda A, Kawakami O, Dohmoto Y, Takenaka T, 1987. Lanthanide tetrad effects in nature: two mutually opposite types, W and M. Geochem J 21: 119–124

McLing T, Smith W, Smith R, 2014. Utilizing Rare Earth Elements as Tracers in High TDS Reservoir Brines in CCS Applications. Energy Procedia 63 (2014) 3963 – 3974

Masuda A. Ikeuchi Y., 1979. Lanthanide tetrad effect observed in marine environment. Geochem. J. 13, 19-22.

Matter, J.M., Takahashi, T., Goldberg, D., 2007. Experimental evaluation of in situ CO2–water–rock reactions during CO2 injection in basaltic rocks: implications for geological CO2 sequestration. Geochemistry, Geophysics, Geosystems 8 (2), 1–19.

Michard, A., 1989. Rare earth element systematics in hydrothermal fluids. Geochim. Cosmochim. Acta 53, 745–750.

Millero, F.J., 1992. Stability constants for the formation of rare earth inorganic complexes as a function of ionic strength. Geochimica Cosmochimica Acta 56, 3123–3132.

Monecke T., Kempe U., Monecke J., Sala M., Wolf D., 2002. Tetrad effect in rare earth element distribution patterns: a method of quantification with application to rock and mineral samples from granite-related rare metal deposits. Geochimica et Cosmochimica Acta, 66,7,1185-1196

Munemoto T., Ohmori K., Teruki I 2015. Rare earth elements (REE) in deep groundwater from granite and fracture-filling calcite in the Tono area, central Japan: Prediction of REE fractionation in paleo- to present-day groundwater, Chemical Geology 417, 58-67

Negrel P., Guerrot C. , Cocherie A., Azaroual M. , Brach M. , Fouillac C., 2000. Rare earth elements, neodymium and strontium isotopic systematics in mineral waters: evidence from the Massif Central, France. Applied Geochemistry 15, 1345-1367

Noack, C.W., Dzombak, D.A. and Karamalidis, A.K., 2014. Rare earth element distributions and trends in natural waters with a focus on groundwater. Environ. Sci. Technol. 48, 4317-4326.

Nordstrom, D.K., Plummer, L.N., Langmuir, D., Busenberg, E., May, H.M., Jones, B.F., Parkhurst, D.L., 1990. Revised Chemical Equilibrium Data for Major Water-mineral Reactions and Their Limitations.

Odin B., Conrad G. 1987. Les cinérites, marqueurs asequentiels au sein de la sedimentation permienne, continentale et ryhtmique, du basin de Lodeve (Herault, France). Annales de la Société géologique de Belgique, T.110, 271-278

Ohta, A., H. Kagi, M. Nomura, H. Shitsuno, and I. Kawabe, 2009, Coordination study of rare earth elements on Fe oxyhydroxide and Mn dioxides: Part ii. Correspondence of structural change to irregular variations of partitioning coeffcients and tetrad effect variations appearing in interatomic distances, Am. Mineral., 94 (4), 476–486.

Ohta A., Kawabe I., 2001. REE(III) adsorption onto Mn dioxide (δ-MnO2) and Fe oxyhydroxide: Ce(III) oxidation by δ-MnO2. Geochimica et Cosmochimica Acta, 65, 5, 695-703

Parkhurst, D.L., Appelo, C.A.J., 2013. Description of input and examples for PHREEQC version 3-a computer program for speciation, batch-reaction, one-dimensional transport, and inverse geochemical calculations. U. S. Geol. Surv. Tech. methods, book 6, 497.

Pérez-López R. , Delgado J., Nieto J.M., Márquez-García B.(2010). Rare earth element geochemistry of sulphide weathering in the São Domingos mine area (Iberian Pyrite Belt): a proxy for fluid–rock interaction and ancient mining pollution. Chem. Geol., 276, 29-40

Pearce J.K, Kirste D.M., Dawson G.K.W. ; Farquhar S.M., Biddle D., Golding S.D., Rudolph V., 2015. SO2 impurity impacts on experimental and simulated CO2–water–reservoir rock reactions at carbon storage conditions. Chemical Geology,399, 65-86

Perry E. P., Gysi A.P., 2018. Rare Earth Elements in Mineral Deposits: Speciation in Hydrothermal Fluids and Partitioning in Calcite. Geofluids Volume 2018, Article ID 5382480, 19 pages https://doi.org/10.1155/2018/5382480Pourret, O., Davranche, M., Gruau, G., Dia, A., 2007a. Rare earth elements complexation with humic acid. Chem. Geol. 243, 128–141.

Pourret O., Dia A., Davranche M., Gruau G., Hcheel. 24Ang,e M.,2007b. Organo-colloidal control on major- and trace-element partitioning in shallow groundwaters: Confronting ultrafiltration and modelling. Applied Geochemistry 22 (2007) 1568ellin

Pourret, O., Martinez, R.E., 2009. Modeling lanthanide series binding sites on humic acid. J. colloid interface Sci. 330 (1), 45–50.

Pourret, O., Gruau, G., Dia, A., Davranche, M., Molenat, J., 2010. Colloidal control on the distribution of rare earth elements in shallow groundwaters. Aquat. Geochem. 16 (1), 31.

Pourret O., Tuduri J. 2017. Continental shelves as potential resource of rare earth elements, Scientific Reports, 7 :5857

Qu, C. L., Liu, G., and Zhao, Y. F. 2009. Experimental study on thefractionation of yttrium from holmium during the coprecipita-tion with calcium carbonates in seawater solutions, Geochem. J., 43, 403–414

Quinn, K.A., Byrne, R.H., Schijf, J., 2006. Sorption of yttrium and rare earth elements by amorphous ferric hydroxide: influence of solution complexation with carbonate. Geochimica Cosmochimica Acta 70 (16), 4151–4165

Quinn, K.A., Byrne, R.H., Schijf, J., 2007. Sorption of yttrium and rare earth elements by amorphous ferric hydroxide: influence of temperature. Environ. Sci. Technol. 41 (2), 541–546.

Rillard, J., Gombert, P., Toulhoat, P., Zuddas, P., 2014. Geochemical assessment of CO2 perturbation in a shallow aquifer evaluated by a push–pull field experiment. International Journal of Greenhouse Gas Control 21, 23–32.

Shabani M.B., Akagi T., Masuda A., 1992. Preconcentration of trace rare-earth elements in seamater by complexation with bis(2-ethylhexyl) hydrogen phosphate adsorbed on a C18 cartridge and determination by inductively coupled plasma mass spectrometry. Analytical Chemistry, 64(7), 737-743

Shand P., Johannesson K.H., Chudaev O. V., Chudaeva V. , Edmunds W. M., 2005. Rare Earth Element Contents of High pCO2 Groundwaters of Primorye, Russia: Mineral Stability and complexation Controls. In book: Rare Earth Elements in Groundwater Flow Systems, DOI: 10.1007/1-4020-3234-X_7

Shannon, R.T., 1976. Revised effective ionic radii and systematic studies of interatomic distances in halides and chalcogenides. Acta Crystallogr. Sect. A Cryst. Phys. Diffr. Theor. general Crystallogr. 32 (5), 751–767.Schijf, J., Marshall, K.S., 2011. YREE sorption on hydrous ferric oxide in 0.5 M NaCl solutions: a model extension. Mar. Chem. 123 (1), 32–43.

Schijf, J., Byrne, R.H., 2004. Determination of SO4 β1 for yttrium and the rare earth elements at I=0.66 m and t=25 ºC-implications for YREE solution speciation in sulfate-rich waters. Geochimica cosmochimica acta 68 (13), 2825–2837.

Sholkovitz, E. R., 1995, The aquatic chemistry of rare earth elements in rivers and estuaries, Aquat. Geochem.,1(1), 1–34

Shu X., , Liu Y., 2019. Fluid inclusion constraints on the hydrothermal evolution of the Dalucao Carbonatite-related REE deposit, Sichuan Province, China. Ore Geology Reviews 107, 41–57

Siirila, E.R., Navarre-Sitchier, A., Maxwell, R.M., McCray, J.E., 2012. A quantitative methodology to assess the risks to human health from CO2 leakage into groundwater, Advances Water Resources 36, 146-164.

Steinmann, M. and Stille, P., 2008. Controls on transport and fractionation of the rare earth elements in stream water of a mixed basaltic-granitic catchment (Massif Central, France). Chem. Geol. 254, 1-18.

Takahashi Y., Yoshida H., Sato N., Hama K., Yusa Y., Shimizu H., 2002. W- and M-type tetrad effects in REE patterns for water–rock systems in the Tono uranium deposit, central Japan. Chemical Geology 184, 311 – 335

Takahashi Y., Yamamoto M., Yamamoto Y., Tanaka K. 2010. EXAFS study on the cause of enrichment of heavy REEs on bacterial cell surfaces. Geochimica et Cosmochimica Acta 74,5443–5462

Tang, J., Johannesson, K.H., 2003. Speciation of rare earth elements in natural terrestrial waters: assessing the role of dissolved organic matter from the modeling approach. Geochimica Cosmochimica Acta 67 (13), 2321–2339.

Tostevin, R., Shields, G. A., Tarbuck, G. M., He, T., Clarkson, M. O., & Wood, R. A. (2016). Effective use of cerium anomalies as a redox proxy in carbonate-dominated marine settings. Chemical Geology, 438, 146-162.

Vahidi E., Navarro J., Zhao F., 2016. An initial life cycle assessment of rare earth oxides production from ion-adsorption clays. Resources, Conservation and Recycling. 113, 1–11

Verplanck, P.L., Nordstrom, D.K., Taylor, H.E., Kimball, B.A., 2004. Rare earth element partitioning between iron oxyhydroxides and acid mine waters. Appl. Geochem. 19, 1339–1354.

Wilkin, R.T., Digiulio, D.C., 2010. Geochemical impacts to groundwater from geologic carbon sequestration: controls on pH and inorganic carbon concentrations from reaction path and kinetic modeling. Environmental Science & Technology 44, 4821-4827.

Wood, S.A., 1990. The aqueous geochemistry of the rare-earth elements and yttrium: 1. Review of available low-temperature data for inorganic complexes and the inorganic REE speciation of natural waters. Chem. Geol. 82, 159–186.

Worrall, F. and Pearson, D.G. (2001) Water-rock interaction in an acidic mine discharge as indicated by rare earth element patterns. Geochim. Cosmochim. Acta 65, 3027-3040.

Wunsch, A., Navarre-Sitchler, A.K., Moore, J., Ricko, A., McCray, J.E., 2013. Metal release from dolomites at high partial-pressures of CO2. Applied Geochemistry 38, 33–47.

Yang, J., Verba, C., Torres, M., Hakala, J.A., Empirically assessing the potential release of rare earth elements from black shale under simulated hydraulic fracturing conditions, Journal of Natural Gas Science & Engineering (2018), doi: 10.1016/j.jngse.2017.09.011.

Zwahlen C.. , Cathy Hollis C. , Lawson M., Becker S.P., Boyce A., Zhou Z., Holland G. (2019). Constraining the fluid history of a CO2 ‐ H2S reservoir: Insights from stable isotopes, REE, and fluid inclusion microthermometry. Geochemistry, Geophysics, Geosystems, 20, 359–382. https://doi.org/10.1029/2018GC007900
.

872
873
874
875
876
877
878
879

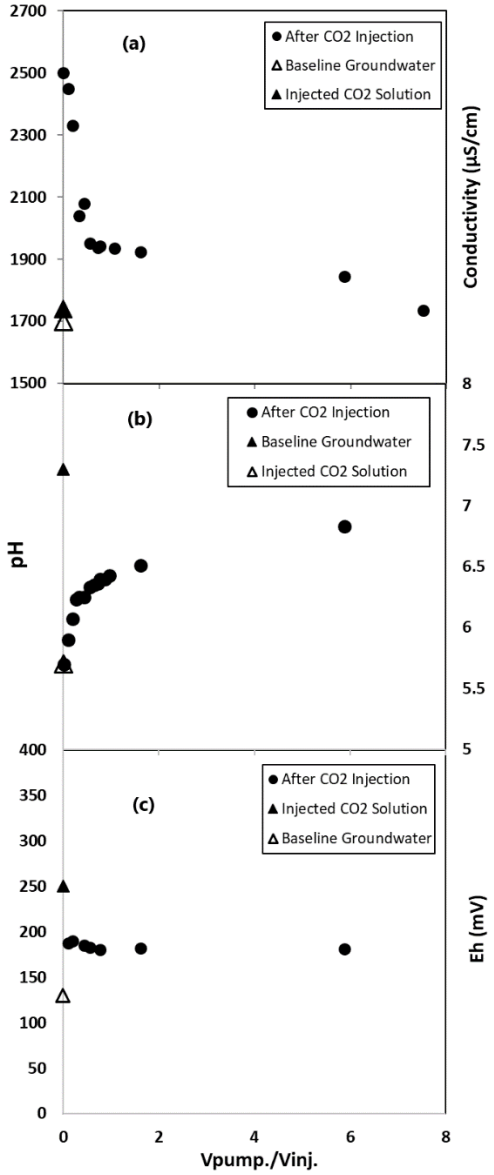

Fig. 1: (a) Conductivity (µS/cm) of groundwater as a function of a function of the ratio pumped (Vp.) volume to injection volume (Vinj.). Values are indicated for baseline groundwater, injected CO_2 solution and groundwater re-pumped after CO_2 injection; (b) pH values as a function of ratio Vp./Vinj.; (c) Redox potential (Eh in mV) measured as a function of ratio Vp./Vinj.

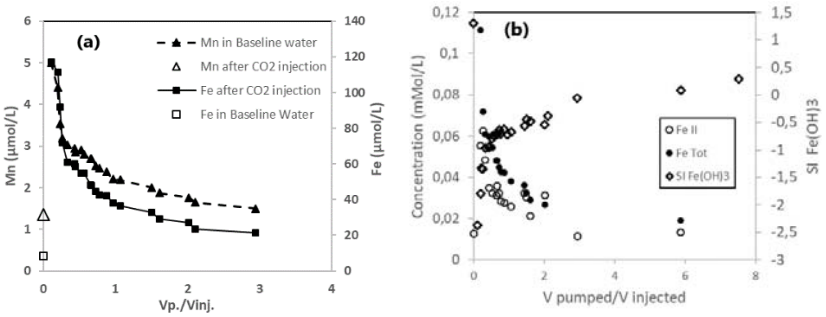

Fig. 2 : (a) Molar concentration (µmol/L) of dissolved iron (Fe, right axis) and manganese (Mn, left axis) as a function of the ratio pumped volume (Vp.) to injection volume (Vinj.);(b) Molar concentration (mMol/L) of total dissolved iron (Fe Tot, left axis), iron two Fe2+ (Fe II) and Saturation Index in Ferrihydrite Fe(OH)3 (left axis)as a function of ratio Vp./Vinj. Figure (b) is extracted from Rillard et al 2014.

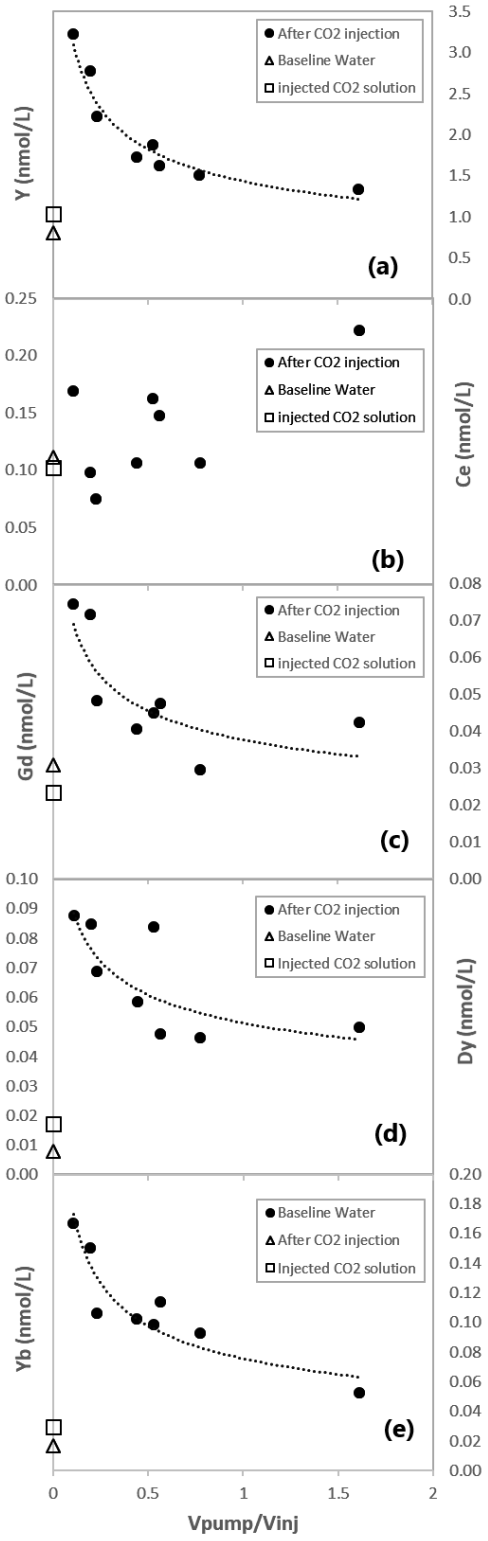

Fig. 3: (a) Molar concentration (nmol/L) in yttrium as function of the ratio pumped volume (Vp.) to injection volume (Vinj.), representative of HREE group; (b) Cerium concentration as a function of Vp./Vinj. ratio, representative of LREE group; (c) Gadolinium concentration (nmol/L) as a function of ratio Vp./Vinj. representative of MREE group; (d) Dysprosium concentration (nmol/L) as a function of

ratio Vp./Vinj. representative of MREE group; (e) Ytterbium concentration (nmol/L) as function of ratio Vp./Vinj. representative of HREE group.

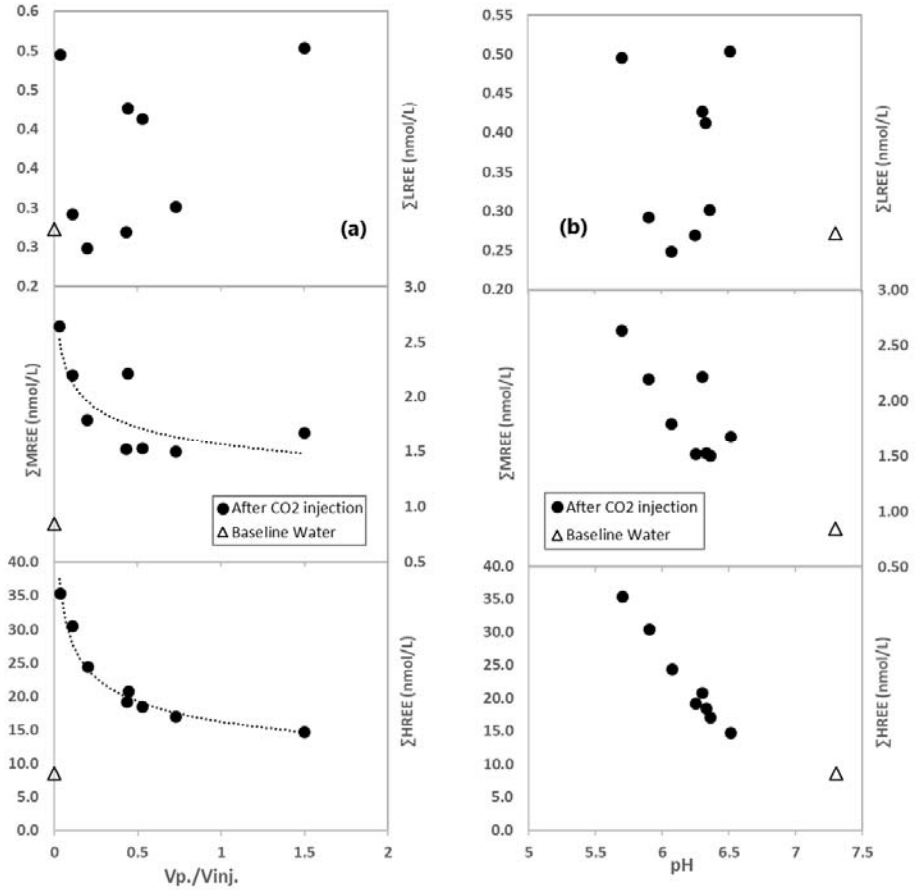

Fig. 4 : (a) Sum of LREE (La, Ce, Pr, Sm), MREE (Eu, Gd, Tb, Dy, Ho), HREE (Er, Tm, Yb, Lu, Y) as function of the ratio pumped volume (Vp.) to injection volume (Vinj.) ; (b) Sum of LREE (La, Ce, Pr, Sm), MREE (Eu, Gd, Tb, Dy, Ho), HREE (Er, Tm, Yb, Lu, Y) as function of pH

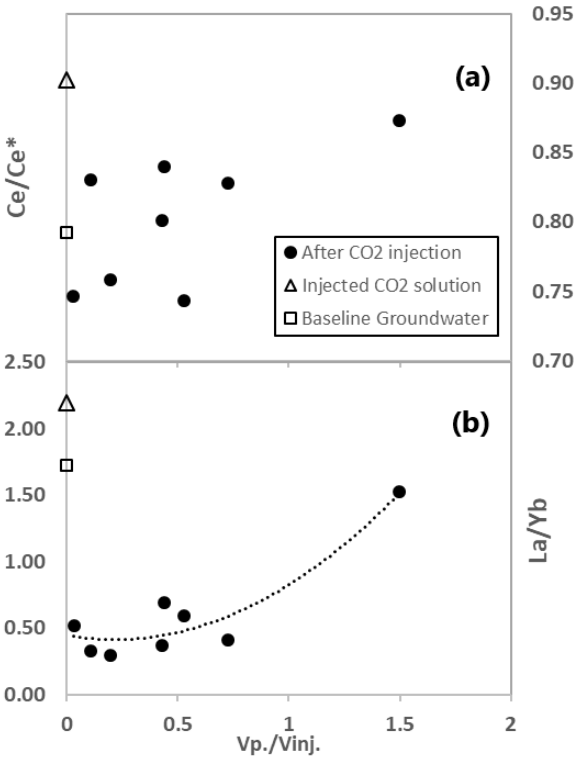

Fig. 5 : (a) Cerium anomaly Ce/Ce* as a function of the ratio pumped volume (Vp.) to injection volume (Vinj.); (b) La/Yb ration as a function of the ratio pumped volume (Vp.) to injection volume (Vinj.)

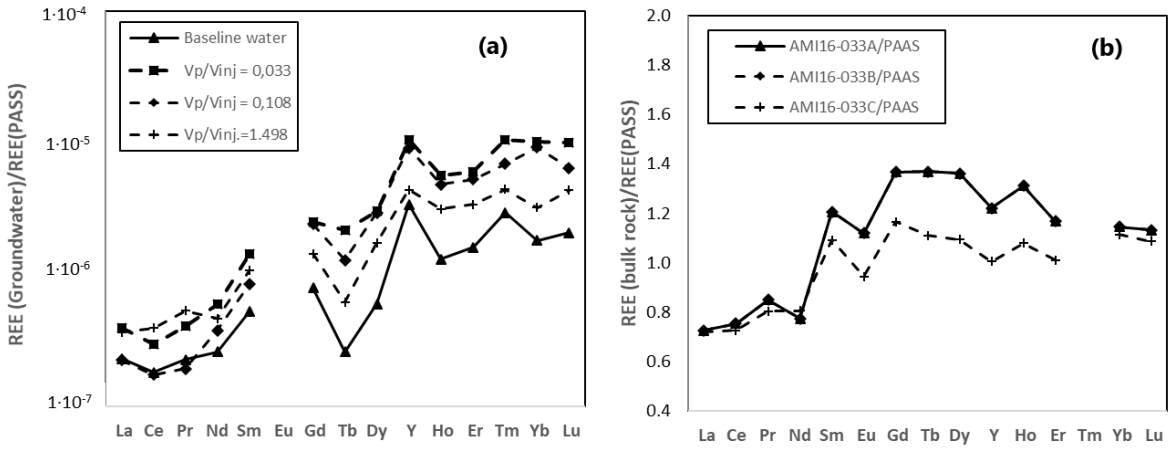

Fig. 6: (a) Dissolved REE concentrations in groundwater samples normalized to Post Archean Australian Shale (PAAS), four representative samples are illusatrated (baseline groundwater, Vp/Vinj. = 0.033, Vp/Vinj=0.108, Vp/Vinj=1.498); (b) REE concentrations in bulk rock samples normalized to Post Archean Australian Shale (PAAS), data issued from Chopin (2016).

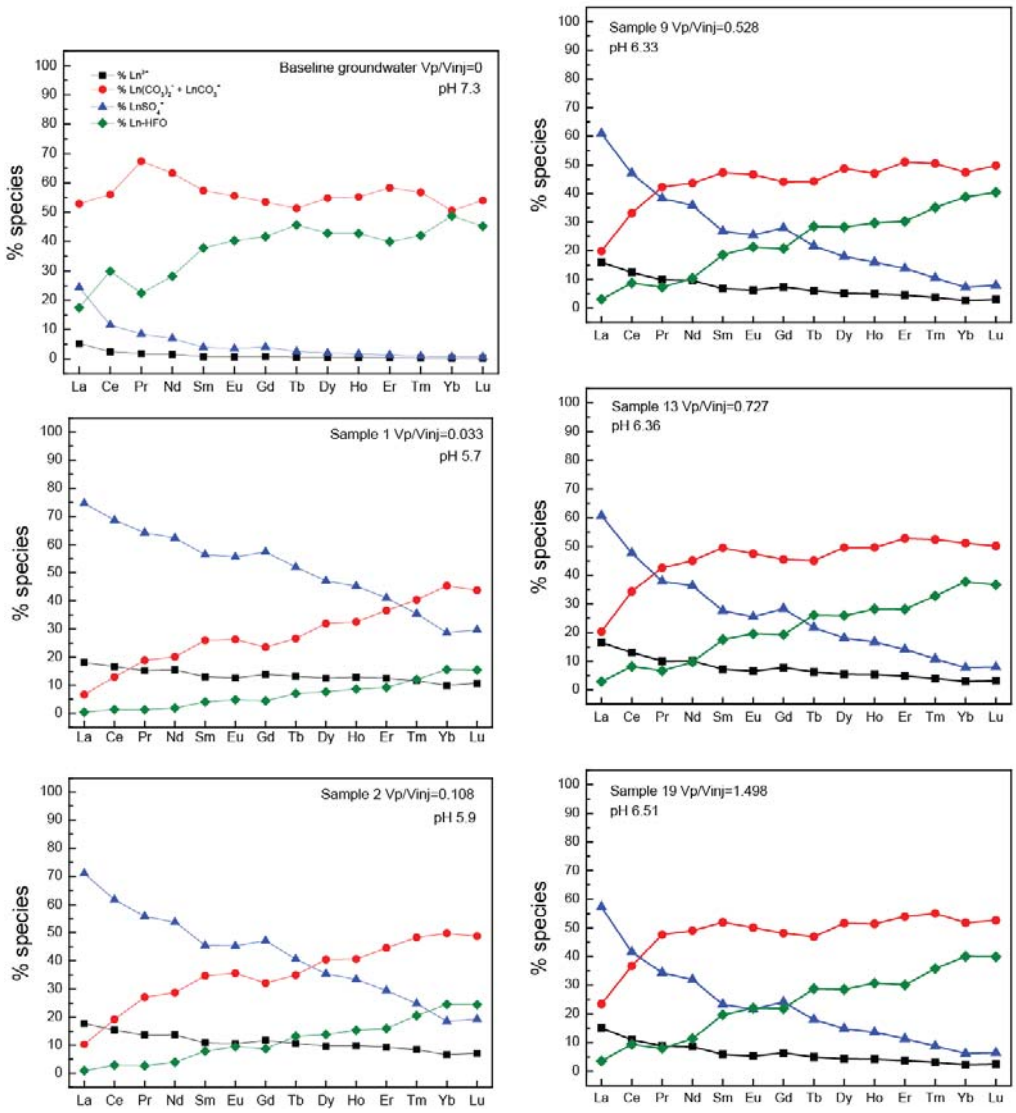

Fig. 7 : Proportion (%) of Ln-Carbonate, Ln-Sulphate, Ln-iron oxihydroxide complex and free Ln^{3+} calculated by the geochemical model in sample Baseline Water, and selected samples following CO_2 injection (Sample 1, Sample 2, Sample 9 , Sample 13, Sample 19). The pH values and Vp/Vinj ratio of each individual sample are indicated in the diagrams.

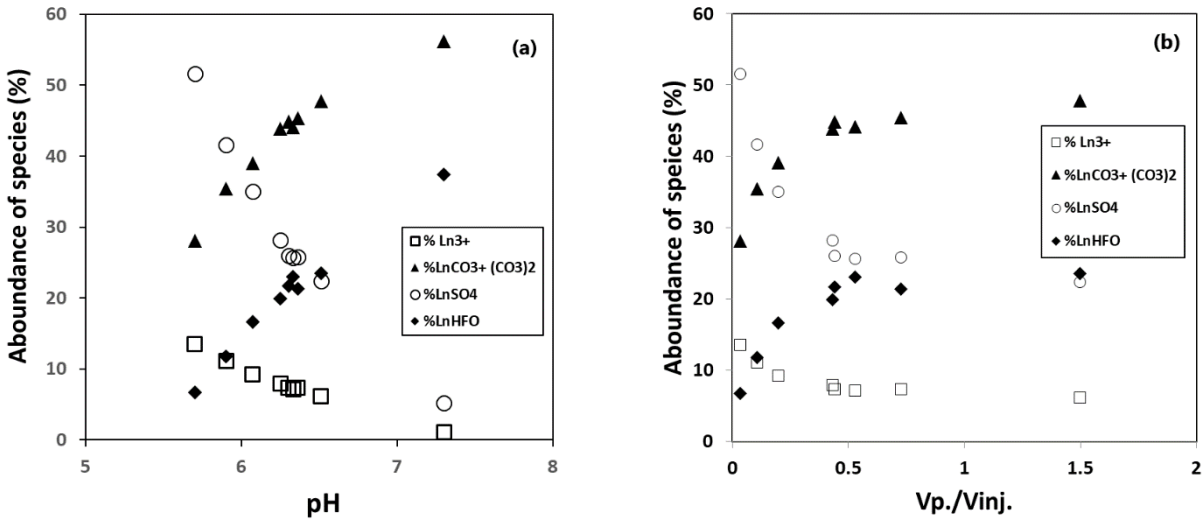

Fig.8: Total proportion (%) of Ln-Carbonate, Ln-Sulphate, Ln-iron oxihydroxide complex and free Ln^{3+} calculated by the geochemical model as a function of (a) pH and (b) the ratio pumped volume (Vp.) to injection volume (Vinj.)

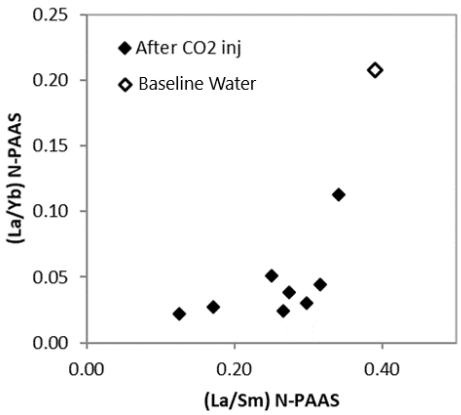

Fig. 9: La/Yd ratio as a function of La/Sm ratio (normalized to PAAS)

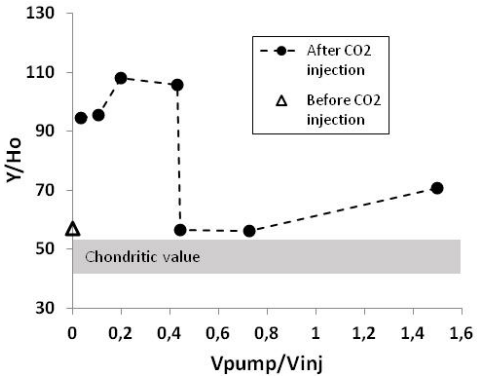

Fig.10: Y/Ho molar ratio as a function of Vpump./Vinj. ratio. Groundwater composition before CO_2 injection is represented by white triangle.

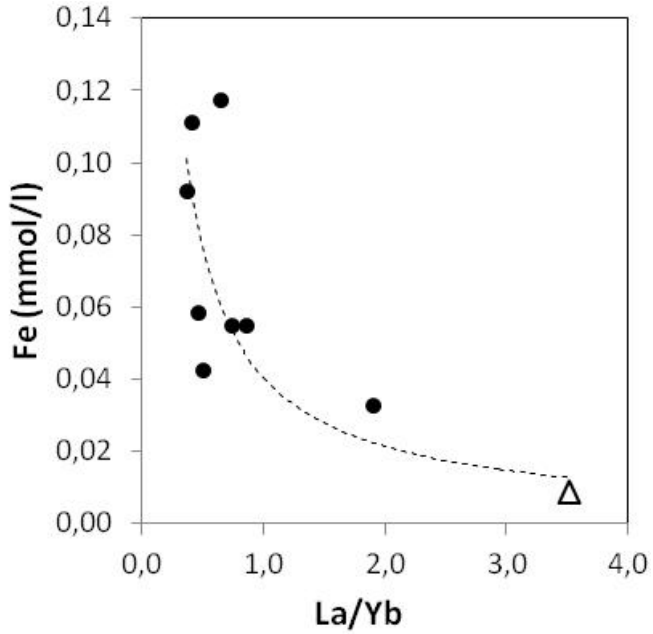

Fig.11: Molar concentration in dissolved iron (mmol/l) as a function of La/Yb ratio. Groundwater composition before CO_2 injection is represented by white triangle.